Performance of Hyperelastic Material Laws in Simulating Biaxial Deformation Response of Polypropylene and High Impact Polystyrene

K. Y. Tshai, E. M. A. Harkin-Jones and P. J. Martin

Abstract Free surface moulding processes such as thermoforming and blow moulding involve thermal and spatial varying rate dependent biaxial deformation of polymer. These processes are so rapid that the entire forming took place in a matter of seconds. As a result of the elevated rate of deformation, assumption that the deforming polymers experience no time dependent viscous dissipation or perfectly elastic up to large strain has became a common practice in numerical simulation. Following the above assumption, *Cauchy's* elastic and hyperelastic theories, originally developed for vulcanised natural rubber has been widely used to represent deforming polymeric materials in free surface moulding processes. To date, various methodologies were applied in the development of these theories, the most significant are those develop purely based on mathematical interpolation (mathematical models) and a more scientific network theories that involves the interpretation of macro-molecular structure within the polymer. In this chapter, the most frequently quoted *Cauchy's* elastic and hyperelastic theories, including Ogden, Mooney–Rivlin, neo-Hookean, 3-chain, 8-chain, Van der Waals full network, Ball's tube model, Edwards–Vilgis crosslinks-sliplinks model and the elastic model of Sweeney–Ward are reviewed. These models were analysed and fitted to a series of experimental high strain rate, high temperature, biaxial deformations data of polypropylene (PP) and high impact polystyrene (HIPS). The performance and

K. Y. Tshai (✉)
Department of Mechanical, Materials and Manufacturing Engineering,
University of Nottingham Malaysia Campus, Jalan Broga, 43500
Semenyih, Selangor, Malaysia
e-mail: Kim-Yeow.Tshai@nottingham.edu.my

E. M. A. Harkin-Jones · P. J. Martin
School of Mechanical and Aerospace Engineering, Queen's University Belfast,
Ashby Building, Stranmillis Road, Belfast BT9 5AH, Northern Ireland, UK
e-mail: e.harkinjones@qub.ac.uk

P. J. Martin
e-mail: p.j.martin@qub.ac.uk

suitability of the various models in capturing the polymer's complex deformation behaviour during free surface moulding processes is presented.

Keywords Hyperelastic model · Biaxial deformation · High strain rate · High temperature · Free surface moulding

1 Introduction

Free surface moulding processes such as thermoforming and blow moulding are employed extensively in the food packaging industry, automobile applications, medical devices and most of our dairy appliances. It is widely recognised that this process is not utilised to its full potential. Optimisation of these processes are becoming technically challenging as newer process variations, materials, tighter sheet/preform and part tolerances, more critical applications and sophisticated controls are developed. At present, trial and error method is still widely practiced among small to medium manufacturing industries. Clearly a more scientific, efficient and sensible technique is required to reduce the excessive lead time and investment costs incurred during embodiment and detail design. To achieve these aims, the use of computer simulations to predict material behaviour under various processing conditions appears to be a very powerful tool. However, for these simulations to be useful it is important to integrate the analysis with an accurate material model. Utilising a high precision model simulating the material behaviour under actual forming conditions capable of effectively optimise the processing conditions as well as forming deployment, wall thickness, part shape and dimensional stability of the final part. In this chapter, the most frequently quoted *Cauchy's* elastic and hyperelastic theories, including Ogden, Mooney–Rivlin, neo-Hookean, 3-chain, 8-chain, Van der Waals full network, Ball's tube model, Edwards–Vilgis crosslinks-sliplinks model and the elastic model of Sweeney–Ward are reviewed. These models were analysed and fitted to a series of experimental high strain rate, high temperature, biaxial deformations data of polypropylene (PP) and high impact polystyrene (HIPS). The performance and suitability of the various models in capturing the polymer's complex deformation behaviour during free surface moulding processes is presented.

2 Experimental

2.1 Material

The thermoplastics tested in this work were pre-extruded HIPS sheet consisting white pigment (single batch production graded as Atofina ATO DPO 02) and nucleated, non-pigmented semi-crystalline isotactic homopolymer PP sheet with
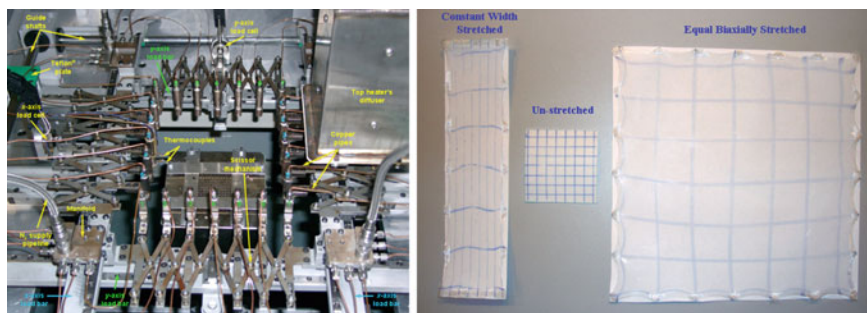
Fig. 1 Queen's biaxial stretcher (*left*); CW, un-stretched and EB stretched specimen (*right*)

anti-static agent (graded as Appryl 3030 BT1). The HIPS sheet has an average thickness of 1.51 ± 0.01 mm and MFI as quoted by the company was 4.5 (200 °C/ 5 kg, g/10 min) while the PP sheets has an average thickness of 1.42 ± 0.01 mm, MFI of 3 (230 °C/2.16 kg, g/10 min) and weight average molecular weight M_w as obtained by gel permeation chromatography was 339,000. The crystallinity and peak melting temperature of the PP sheet as characterised through DSC at heating rate of 10 °C/min were 59.6 % and 165 °C, respectively.

2.2 Biaxial Test

Equal biaxial (EB) and constant width (CW) deformation tests were carried out with the aids of a biaxial stretcher available at Queen's University Belfast. The pre-extruded specimens were tested under high nominal strain rates (ranging from 2 to 10 s^{-1}) and elevated temperatures (ranging from 145 to 160 °C for PP and 120 to 135 °C for HIPS). The un-stretched samples had a dimension 76×76 mm square and were pre-marked with 10×10 mm square ink grid to facilitate investigation of the local deformation on the post-stretched sample. Figure 1 shows the clamping frame of the biaxial stretcher and a comparison of the final shape obtained from CW and EB to that of an un-stretched sample.

3 Constitutive Modelling of Materials

In the history of material modelling, various constitutive equations were proposed in an attempt to represent the behaviour of particular polymer types depending on their morphological structure, i.e. amorphous or semi-crystalline. Within the literature, the available constitutive material models generally can be categorised into two major groups, hyperelastic and viscoelastic material laws. This chapter mainly concerned on the most frequently quoted *Cauchy's* elastic and hyperelastic theories, including Ogden, Mooney-Rivlin, neo-Hookean, 3-chain, 8-chain, Van

der Waals full network, Ball's Tube model, Edwards-Vilgis crosslinks-sliplinks model and the elastic model of Sweeney-Ward.

3.1 Early Development of Classical Linear Elasticity

Robert Hooke 1678 [1], proposed the well-known Hooke's law of elasticity. For a perfectly elastic Hookean material, the applied force, F (hence stress) acting on its body is directly proportional to the extension, u (hence strain), with the inclusion of a material constant, k (this constant was later identified as the elastic or Young's modulus by Thomas Young in 1807 [2]), given as:

$$F = k \cdot u \tag{1}$$

French mathematician Augustin Cauchy 1789–1857 [3–6] subsequently generalised Hooke's law into three-dimensional elastic bodies and stated that the six components of stress are linearly related to the six components of strain, most commonly known as the constitutive Cauchy's elastic stress-strain relationship. The Cauchy's elastic stress-strain relationship written in the general form as:

$$\begin{bmatrix} \sigma_{11} \\ \sigma_{22} \\ \sigma_{33} \\ \sigma_{12} \\ \sigma_{13} \\ \sigma_{23} \end{bmatrix} = \begin{bmatrix} C_{1111} & C_{1122} & C_{1133} & C_{1112} & C_{1113} & C_{1123} \\ C_{2211} & C_{2222} & C_{2233} & C_{2212} & C_{2213} & C_{2223} \\ C_{3311} & C_{3322} & C_{3333} & C_{3312} & C_{3313} & C_{3323} \\ C_{1211} & C_{1222} & C_{1233} & C_{1212} & C_{1213} & C_{1223} \\ C_{1311} & C_{1322} & C_{1333} & C_{1312} & C_{1313} & C_{1323} \\ C_{2311} & C_{2322} & C_{2333} & C_{2312} & C_{2313} & C_{2323} \end{bmatrix} \begin{bmatrix} \varepsilon_{11} \\ \varepsilon_{22} \\ \varepsilon_{33} \\ \varepsilon_{12} \\ \varepsilon_{13} \\ \varepsilon_{23} \end{bmatrix} \tag{2}$$

where $[C_{ijkl}]$ is the constitutive stiffness matrix. There are 36 matrix components in general but conservative elastic materials possess a strain energy for a given strain state, as such, the constitutive stiffness matrix $[C_{ijkl}]$ is symmetric (i.e. $C = C^T$, only 21 independent matrix components in the generalised *Hooke's* law).

Taking the stress components as σ_{ij} and strain components as ε_{ij}, if three planes of symmetry exist and if the coordinate planes are parallel to these planes, the Cauchy's elastic stress-strain relationship can be organised into a simpler form, given as:

$$\begin{bmatrix} \sigma_{11} \\ \sigma_{22} \\ \sigma_{33} \\ \sigma_{12} \\ \sigma_{13} \\ \sigma_{23} \end{bmatrix} = \begin{bmatrix} C_{1111} & C_{1122} & C_{1133} & 0 & 0 & 0 \\ C_{1122} & C_{2222} & C_{2233} & 0 & 0 & 0 \\ C_{1133} & C_{2233} & C_{3333} & 0 & 0 & 0 \\ 0 & 0 & 0 & C_{1212} & 0 & 0 \\ 0 & 0 & 0 & 0 & C_{1313} & 0 \\ 0 & 0 & 0 & 0 & 0 & C_{2323} \end{bmatrix} \cdot \begin{bmatrix} \varepsilon_{11} \\ \varepsilon_{22} \\ \varepsilon_{33} \\ \varepsilon_{12} \\ \varepsilon_{13} \\ \varepsilon_{23} \end{bmatrix} \tag{3}$$

where the stiffness coefficient C_{ijkl} is a fourth order tensor (denoting the ratio of stress to strain) with only 9 independent coefficients and the material is referred as orthotropic symmetric.

While the generalised Hooke's law is capable of describing deformation of a material within its linear elastic region, this model failed to simulate the non-linear, large deformation behaviour of polymeric materials. To overcome this limitation, various forms of constitutive equations have been proposed and this has led to the development of a number of non-linear elastic or hyperelastic models. The fundamental concept of these formulations is generally based on the conservation of energy. The theory states that any work done (in a reversible isothermal process) in the deformation of a material is stored as potential energy (frequently called the free energy potential or strain energy) within the deforming body, and a deformed material will completely recover to its initial un-stretched state on removal of the forming force. In other words, the nonlinear strain energy for a given strain state only depends on the strain state itself and not on the manner in which this strain state was obtained. The many forms of nonlinear strain energy function W generally can be categorised into two major groups depending on the fundamental concepts employed in their development, namely phenomenological and physical network hyperelastic material laws.

3.2 Phenomenological Hyperelastic Material Laws

3.2.1 Mooney-Rivlin Model

Within the many forms of phenomenological strain energy functions, the earliest and simplest is the *Mooney* form. Assuming a material is incompressible and isotropic, Mooney 1940 [7] derived by purely mathematical arguments, a representation of the strain energy, W.

$$W = C_1\left(\lambda_1^2 + \lambda_2^2 + \lambda_3^2 - 3\right) + C_2\left(\lambda_1^{-2} + \lambda_2^{-2} + \lambda_3^{-2} - 3\right) \qquad (4)$$

and

$$\lambda_i = \frac{L_i + \Delta L_i}{L_i} \qquad (5)$$

where λ_i ($i = 1,2,3$) are the principal stretch ratios given as the ratio of current length ($L + \Delta L$) over the original length L in the three principal directions respectively, C_1 and C_2 are two elastic constants.

Once the strain energy function W has been defined, assuming that the material is incompressible, the principal true stresses σ_T can be computed (by differentiating W with respect to each of the three principal stretch ratios, $i = 1,2,3$) from W to within an arbitrary pressure, P, where P can usually be determined from the

boundary conditions (in order to eliminate the pressure term, the true stress-stretch ratio relations are frequently written in terms of the difference in two principal stresses, i.e. $\sigma_1 - \sigma_2$, $\sigma_2 - \sigma_3$ and $\sigma_3 - \sigma_1$):

$$(\sigma_T)_i = \lambda_i \cdot \frac{\partial W}{\partial \lambda_i} + P \qquad (6)$$

Eight years later in 1948, Rivlin [8, 9] claimed that the strain energy function W should be formulated such that it is symmetrical with respect to the three principal stretch ratios for the principle of material objectivity to be satisfied. In this context, the author proposed that the strain energy function must depend only on the even powers of the three stretch ratios. This has led to the development of three strain invariants (I_1, I_2, and I_3) as even power functions of λ_i ($i = 1, 2, 3$), representing strain fields that are independent on the particular choice of coordinate system.

$$
\begin{aligned}
I_1 &= \lambda_1^2 + \lambda_2^2 + \lambda_3^2 \\
I_2 &= \lambda_1^2\lambda_2^2 + \lambda_2^2\lambda_3^2 + \lambda_3^2\lambda_1^2 \\
I_3 &= \lambda_1^2\lambda_2^2\lambda_3^2.
\end{aligned}
\qquad (7)
$$

For an incompressible material, the third strain invariant $I_3 = 1$ since $\lambda_1\lambda_2\lambda_3 = 1$, leaving only two independent strain invariants (I_1 and I_2) in the system. The author subsequently proposed the use of only first and second invariants of strain in the strain energy function and stated that this function could be expanded as an infinite series as show below.

$$W = \sum_{i=0,j=0}^{\infty} C_{ij}(I_1 - 3)^i (I_2 - 3)^j \qquad (8)$$

where C_{ij} are material constants with C_{00} being equal to 0.

However, when considering only the first term, the *Rivlin* strain energy function for an incompressible material (Eq. 8) the *Mooney* form is obtained. This is generally known as the first order *Mooney-Rivlin* or simply the *Mooney-Rivlin* relationship for higher order terms.

$$W = C_{10}(I_1 - 3) + C_{01}(I_2 - 3) \qquad (9)$$

3.2.2 Ogden Model

In a slightly later development, Ogden 1972 [10] employed a more formal treatment by formulating the strain energy function directly in terms of the three principal stretch ratios. The author proposed that the 'power (constant α_i in Eq. 10

below)' applied to the three principal stretch ratios may have any values, positive or negative and are not necessarily integers, given in the form below.

$$W = \sum_{i=1}^{N} \frac{2\mu_i}{\alpha_i^2} \left(\lambda_1^{\alpha_i} + \lambda_2^{\alpha_i} + \lambda_3^{\alpha_i} - 3 \right) \tag{10}$$

where μ_i and α_i are material constants determined from the experimental data and $i = 1, 2, 3, \ldots, N$, representing the order of the strain energy function.

It should be noted that under unique case where $N = 1$ and constant $\alpha_i = 2$, the *Ogden* model yields a special case of the *Mooney* form with constant $C_2 = 0$.

3.3 Physical Network Hyperelastic Material Laws

In physical network hyperelastic material laws, polymers are considered as consisting of numerous long flexible chains, each of which is capable of assuming a variety of configurations in response to the thermal vibrations of '*micro-Brownian*' motion of their constituent atoms. Furthermore it is assumed that the molecular chains are interlinked so as to form a coherent network but that the number of cross-links is relatively small and is not sufficient to significantly interfere with the motion of the chains. In the unstrained state, these chain molecules always tend to assume a set of more stable configurations corresponding to a state of maximum entropy. In the case where the chain molecules are constrained by external forces, their configuration will be changed to produce a state of strain. The probability of potential stable chain configurations in the unstrained state has been widely studied using statistical mechanics and assuming that deformation processes at the strained state are always thermodynamically reversible [11, 12].

3.3.1 Gaussian Network Model

neo-Hookean Model

In 1943, Treloar [13, 14] with the assumption that material being incompressible and isotropic, developed the *neo-Hookean* strain energy function by considering the macroscopic molecular configuration of rubber-like materials with *Gaussian* chain length distribution. Since *Gaussian* statistical analysis was the earliest concept used to develop physically based models and this concept is closely related to the development of other physical models, describing this theorem in further detail will provide a better overall picture and aid in the understanding of later developments in this area.

The *Gaussian* network assumes that:

1. The molecular network within a material contains N chains per unit volume, a chain being defined as the segment of a molecule between successive points of cross-linkage.
2. Within a particular chain, there are n 'freely jointed' carbon-carbon (C–C) links/segments, each of length l. The terms freely jointed chain implies that a chain consists of equal C–C links joined together without the restriction that the valence angles should remain constant, a case where random joining or 'random walk' is assumed.
3. The mean-square end-to-end distance for the whole assembly of chains in the unstrained state is the same as for a corresponding set of free chains (end-to-end distance r being very much smaller compared to the fully extended length of the chain).
4. The junction points between chains move on deformation as if they were embedded in an elastic continuum. As a result, the components of length of each chain change in the same ratio as the corresponding dimensions of the bulk rubber, known as 'affine' deformation assumption.
5. The entropy of the network is the sum of the entropies of all individual chains.

Based on the assumptions of a *Gaussian* network, Treloar statistically calculated for a single molecular chain, the number of possible configurations corresponding to a chosen end-to-end distance described in assumption 3 above as well as its entropy. The change in entropy of the whole network was successively computed by the entropy summation of N chains as described in assumption 5. Figure 2 schematically shows a single molecular chain with $n = 36$ freely jointed segments/links of length l, where the probability of the chain assuming end-to-end distance r, according to assumption 3, was statistically evaluated on the basis of spherically symmetrical distribution ($x^2 + y^2 + z^2 = r^2$).

Under a *Gaussian* statistical treatment, the probability that chain end B will fall within an elemental volume between r and dr of a spherical shell of radius r and thickness dr was obtained.

$$P(r) \cdot dr = \frac{b^3}{\pi^{\frac{3}{2}}} \exp\left(-b^2 r^2\right) \cdot 4\pi r^2 \cdot dr \tag{11}$$

where b is a function of both the number of segments/links n and their average length l, given as $b^2 = [3/(2\ nl^2)]$.

By evaluating the most probable value from Eq. 11 (differentiating $p(r)$ with respect to r), it was subsequently found that the mean-square value of r, $(r_{mean})^2$, is $n \cdot l^2$ and thus the un-deformed root-mean-square end-to-end distance, $\left[\sqrt{(r_{mean})^2}\right]$, of any arbitrary molecular chain can be given as $\sqrt{n} \cdot l$. Furthermore it is clear from both *Gaussian* network assumptions and Fig. 2 that the fully stretched length of a freely jointed chain can be given by $n \cdot l$. According to
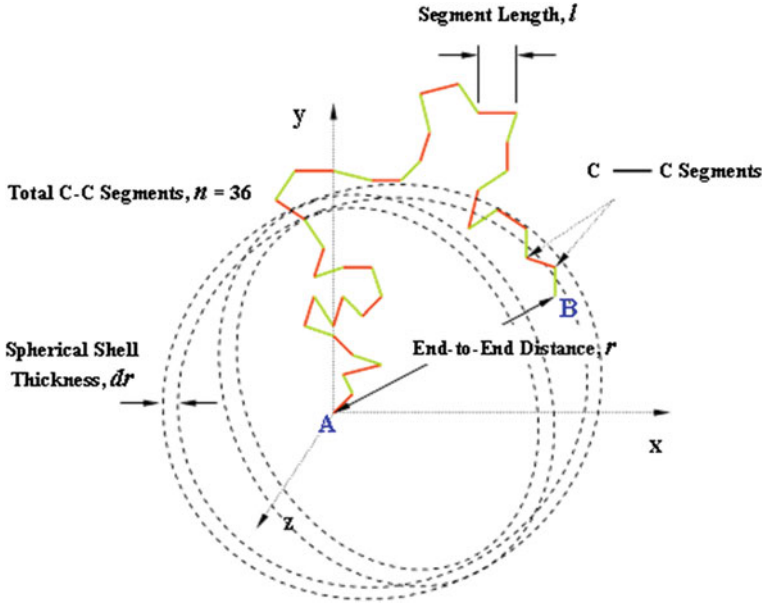
Fig. 2 Single molecular chain with 36 freely jointed segments

Boltzmann's statistical thermodynamics, the entropy of such a freely jointed chain is proportional to the natural logarithm of the number of possible configurations, which in turn can be given in terms of unit volume probability or probability density (e.g. normalised with respect to the spherical shell volume '$4\pi r^2$ '), $p(r)$,

$$s = k_b[\ln p(r)] \tag{12}$$

where k_b is the *Boltzmann's* constant equal to 1.38×10^{-23} JK^{-1}.

Substituting $p(r)$ from Eq. 11 into Eq. 12, a function for the entropy of an undeformed freely jointed chain can be expressed as:

$$s = k_b\left[\ln(c) - b^2 r^2\right] = c - k_b \cdot \left(\frac{3}{2nl^2}\right) \cdot \left(x^2 + y^2 + z^2\right) \tag{13}$$

where c is an arbitrary constant.

On deformation, where the three principal stretch ratios λ_1, λ_2 and λ_3 were chosen to be parallel to the three rectangular axes x, y and z, the entropy of the chain changes to s'.

$$s' = c - k_b \cdot \left(\frac{3}{2nl^2}\right) \cdot \left(\lambda_1^2 x^2 + \lambda_2^2 y^2 + \lambda_3^2 z^2\right) \tag{14}$$

The entropy change on deformation of a single chain was obtained through subtraction ($\Delta s = s' - s$) and the total entropy change for a *Gaussian* network containing N chains can be calculated as:

$$\sum_1^N \Delta s = -k_b \left(\frac{3}{2nl^2}\right) \left[(\lambda_1^2 - 1) \sum_1^N x^2 + (\lambda_2^2 - 1) \sum_1^N y^2 + (\lambda_3^2 - 1) \sum_1^N z^2 \right]$$

(15)

For an isotropic material, there will be no preferential orientation for the x, y or z directions.

$$\sum_1^N x^2 = \sum_1^N y^2 = \sum_1^N z^2 = \frac{1}{3} \sum_1^N r^2$$

(16)

and from *Gaussian* statistical treatment,

$$\sum_1^N r^2 = N \cdot (r_{mean})^2 = N \cdot nl^2$$

(17)

Assuming that the internal energy remains constant on deformation, substitution of Eqs. 16 and 17 into 15 produces the *Helmholtz* free energy for an incompressible, isotropic material under reversible deformation, in terms of the *neo-Hookean* form below.

$$W = -T \cdot \Delta s = \frac{1}{2} N k_b T \left(\lambda_1^2 + \lambda_2^2 + \lambda_3^2 - 3\right)$$

(18)

where $N \cdot k_b \cdot T$ is the material's shear modulus G and T is the absolute temperature.

It should be noted that the strain energy function derived by Treloar (Eq. 18) yields a form of the *Mooney* strain energy function when constant C_2 in Eq. 4 equal to 0.

When fitted the *neo-Hookean* model to experimental data [11], reasonably good agreement was obtained in the low strain region but the model's accuracy gradually decreased with increasing strain. This problem was attributed to the possibility that *Gaussian* distribution function may be valid only as long as the end-to-end distance of the chain is not so large as to be comparable with its fully extended length (generally end-to-end distance r should not be more than 1/3 of the fully extended chain length).

3.3.2 Non-Gausian Network Models

At about the same time as the *neo-Hookean* model was proposed, Kuhn and Grun [15] attempted to describe the probability of the configuration of molecular chains based on a *non-Gaussian* statistical theory. In this study, many assumptions of the *Gaussian* network remained (assumptions 1, 2, 4 and 5) with the exception of the assumption 3 which required the end-to-end distance to be very much less than the fully extended chain length was removed. This was done by replacing the *Gaussian* statistical distribution with an 'inverse *Langevin*' approximation function for the computation of probability distribution. Under inverse *Langevin* statistical analysis, Kuhn and Grun demonstrated that the probability density $p(r)$ for chain end-to-end distance r could be evaluated as:

$$\ln p(r) = c - n\left(\frac{r}{nl}\beta + \ln\frac{\beta}{\sinh\beta}\right) \tag{19}$$

where c is an arbitrary constant and β is a function determined by the fractional extension of the chain *(r/nl)*, given in the form below.

$$\frac{r}{nl} = \coth\beta - \frac{1}{\beta} = \boldsymbol{L}(\beta) \tag{20}$$

The function L is the *Langevin* function and parameter β can be obtained from the inverse of the *Langevin* function L^{-1}, which in turn can be expressed in a series form as shown below:

$$\beta = \boldsymbol{L}^{-1}\left(\frac{r}{nl}\right) = \boldsymbol{L}^{-1}\left(\coth\beta - \frac{1}{\beta}\right) \tag{21}$$

$$\Rightarrow \beta = 3\left(\frac{r}{nl}\right) + \frac{9}{5}\left(\frac{r}{nl}\right)^3 + \frac{297}{175}\left(\frac{r}{nl}\right)^5 + \frac{1539}{875}\left(\frac{r}{nl}\right)^7 + \cdots \tag{22}$$

By substitution of β from Eq. 22 into Eq. 19, the authors obtained a definition for the density $p(r)$, which in turn can be expressed as an expansion series.

$$\ln p(r) = c - n\left[\frac{3}{2}\left(\frac{r}{nl}\right)^2 + \frac{9}{20}\left(\frac{r}{nl}\right)^4 + \frac{99}{350}\left(\frac{r}{nl}\right)^6 + \cdots\right] \tag{23}$$

Adopting an analysis identical to *Boltzmann's* statistical thermodynamics, the entropy of a stretched chain with current end-to-end distance r was obtained as:

$$s = k_b \ln p(r) = c - n \cdot k_b \left[\frac{3}{2}\left(\frac{r}{nl}\right)^2 + \frac{9}{20}\left(\frac{r}{nl}\right)^4 + \frac{99}{350}\left(\frac{r}{nl}\right)^6 + \cdots\right] \tag{24}$$
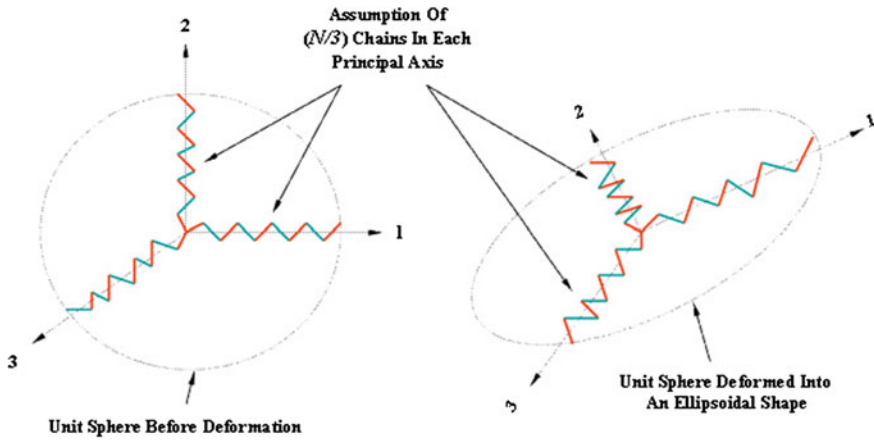
Fig. 3 Network configuration of the three-chain model: noting that the three polymer chains are always oriented in the principal strain axes before and during deformation

For a molecular network containing N chains per unit volume, the total tension of the network can be evaluated as the summation of the differentiated entropy function (with respect to r).

$$f = \sum_{1}^{N} -T\left(\frac{\partial s}{\partial r}\right) = \frac{Nk_bT}{l}\left[3\left(\frac{r}{nl}\right) + \frac{9}{5}\left(\frac{r}{nl}\right)^3 + \frac{297}{175}\left(\frac{r}{nl}\right)^5\right] = \frac{Nk_bT}{l}\boldsymbol{L}^{-1}\left(\frac{r}{nl}\right)$$

(25)

It should be noted that the *Gaussian* formula in Eq. 13 is similar to the first term of Eq. 24 above. This suggested that *Gaussian* statistical theory assumed all higher terms in *(r/nl)* negligible compared to the first term. In the case where the ratio *(r/nl)* increases with increasing chain extension, the prediction from the *Gaussian* distribution function gradually diverges from the 'inverse *Langevin*' statistical treatment, leading to the failure of the *Gaussian* formula at large strain.

Three-Chain Model

The superiority of the *non-Gaussian* over the *Gaussian* statistical theory gave rise to the later development of a network model based on this treatment. Guth et al. [16, 17] who employed a similar concept, developed the three-chain model based on assumption that in a molecular network containing N chains per unit volume *(N/3)* polymer chains per unit volume are always oriented in each of the three principal strain axes such that the system can be represented by 3 identical chains, as shown in Fig. 3.

Therefore, the total network strain energy can be expressed as the sum of the 3 single-chain strain energy functions weighted by the factor $(N/3)$. The three-chain model defined in terms of the principal *Cauchy* stress and stretch ratios relationship can be given as:

$$\sigma_i^{3-chain} = \frac{1}{3}(Nk_bT)\sqrt{n} \cdot \lambda_i \cdot \boldsymbol{L}^{-1}\left(\frac{\lambda_i}{\sqrt{n}}\right) + P \qquad (26)$$

where $(N \cdot k_b \cdot T)$ according to *Gaussian* statistics is a material parameter defining its shear modulus, parameter $(\sqrt{n})$ is a constant obtained from inverse *Langevin* treatment as the ratio of fully extended chain length $(n \cdot l)$ over its initial unstretched length $(\sqrt{n}) \cdot l$, denoted as the 'limiting stretch or finite inextensibility' of the chain λ_{max}. This corresponds to an infinite stress in terms of the model.

Eight-Chain Model

In order to facilitate finite element coding, Arruda and Boyce 1993 [18] developed a simplified form of the full-network model [19–21] where a constitutive relation without the need of numerical integration was developed based on an eight chain representation of the underlying macromolecular network and each individual chain property was described through the use of *non-Gaussian* inverse *Langevin* theory. The proposed model assumed that in a molecular network containing an assembly of N chains per unit volume, each chain consists of n links of length l, there are $(N/8)$ chains per unit volume being arranged in such a way that the system can be represented by 8 identical chains linked at the centre of an enclosed symmetric cube in principal space and their outer ends being fixed at the eight corners of the cube. On deformation, the cube is always oriented in the principal frame and the length of each enclosed chain was evaluated from the three principal stretch ratios λ_1, λ_2, and λ_3 of the cube edges, as shows in Fig. 4.

The eight-chain model defined in terms of the principal *Cauchy* stress and stretch ratios relationship as

$$\sigma_i^{8-chain} = \frac{1}{3}(Nk_bT)\sqrt{n}\frac{\lambda_i^2}{\lambda_{chain}}\boldsymbol{L}^{-1}\left(\frac{\lambda_{chain}}{\sqrt{n}}\right) + P \qquad (27)$$

where material constants (Nk_bT) and $(\sqrt{n})$ as well as the subscript i remain as defined in Eq. 26. The term λ_{chain} is the extension ratio (r/r_0) of the eight chains, defined in terms of the three principal stretch ratios as:

$$\lambda_{chain} = \sqrt{\frac{\lambda_1^2 + \lambda_2^2 + \lambda_3^2}{3}} \qquad (28)$$

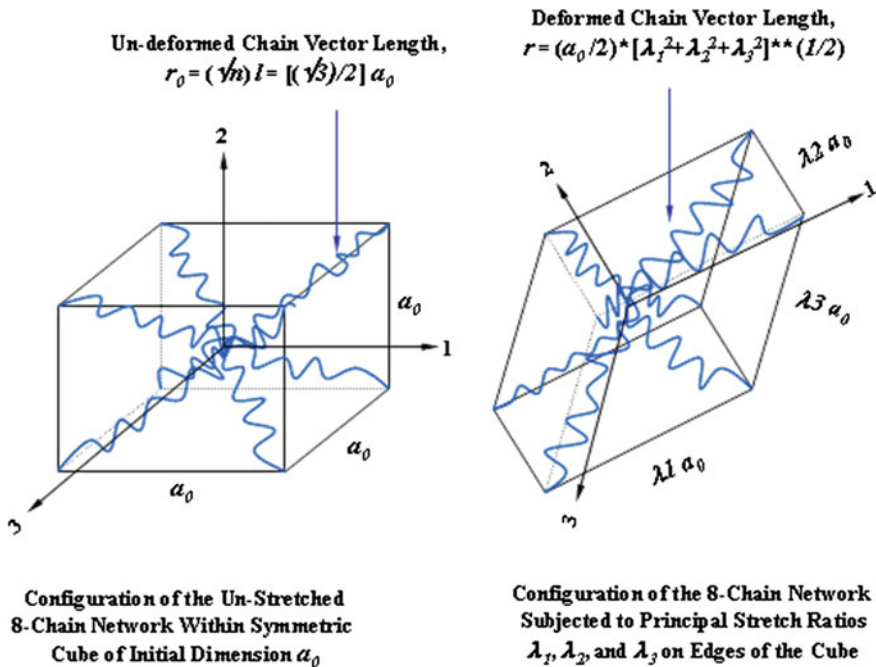where λ_1, λ_2, and λ_3 are the principal stretch ratios of the cube edges.

Un-deformed Chain Vector Length,
$$r_0 = (\sqrt{n})\, l = [(\sqrt{3})/2]\, a_0$$

Deformed Chain Vector Length,
$$r = (a_0/2) \star [\lambda_1^2 + \lambda_2^2 + \lambda_3^2]^{\star\star}(1/2)$$

**Configuration of the Un-Stretched
8-Chain Network Within Symmetric
Cube of Initial Dimension a_0**

**Configuration of the 8-Chain Network
Subjected to Principal Stretch Ratios
$\lambda_1, \lambda_2,$ and λ_3 on Edges of the Cube**

Fig. 4 Schematic diagram of 8-chain model, un-stretched and stretched

Ball "Tube" Model

In agreement with the opinions of Flory and Erman [22], Ball, Edwards and co-
workers [23, 24] claimed that the classical theories of rubber elastic networks [16]
were unrealistic as they assumes the network chains to be held only by numerous
cross-linkages and these molecular chains are capable of moving through each
other as 'phantoms' under the action of external applied forces. However, in a real
polymeric structure, these molecular chains are capable of rotation, bending, and
kinking about their chemical back-bone according to their steric constraints, in
which a large assembly of randomly coiled chains may forms an enormous
entanglement in addition to the cross-linkages afore mentioned. This topological
entanglement gives an additional contribution to the elasticity of rubber and
therefore must be completely preserved in the evaluation for a more physical strain
energy function. The proposed model assumed that in a dense network consisting
of high molecular weight, the motion of two entangled neighbouring chains (each
of which has a fully extended chain length between cross-linkages of L) are
essentially confined in a tube-like region called slip-links, made of the large
number of surrounding molecular chains. A schematic representation of the pro-
posed 'tube model' can be visualised in Fig. 5.
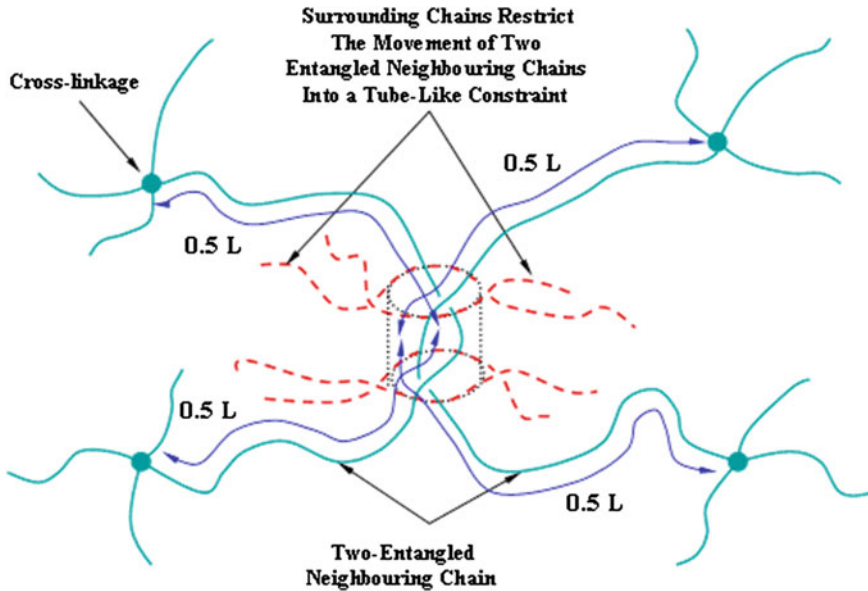
Fig. 5 Schematic representation of 'tube model' consisting of both chain entanglement and cross-linkages as proposed by Ball, Edwards and co-workers

It is clear from Fig. 5 that under the concept of an effective tube of constraint, the sliding freedom of any entangled chains is thus only an arc length 0.5 L in any one direction until it locks onto another entanglement or cross-linkage. Through a rather lengthy treatment of '*replica formalism*', the authors attained a definition for the strain energy, W, of the '*tube* model', involving both the contributions from enormous cross-linkages and chain entanglements. The resulting change in strain energy (per unit volume) can be obtained by integrating the differentiated form (*dW/d*λ) of Eq. 29 below.

$$W = \frac{1}{2}(N_c k_b T) \sum_{i=1}^{3} \lambda_i^2 + \frac{1}{2}(N_s k_b T) \sum_{i=1}^{3} \left[\frac{(1+\eta)\lambda_i^2}{1+\eta\lambda_i^2} + \ln(1+\eta\lambda_i^2) \right] \qquad (29)$$

where parameters N_c and N_s are related to the number of crosslinks and sliplinks per unit volume respectively, k_b is the *Boltzmann's* constant equal to 1.38×10^{-23} JK^{-1}, T is the absolute temperature, η is a measure used to define the freedom to slide for the sliplinks and its value is either greater or equal to 0. In the extreme cases where $\eta = 0$ (equivalent to zero slippage and value L in Fig. 5 equal to 0), the change in strain energy reduces to a state depending only on the contribution from cross-linkages alone.

Van der Waals Model

Employing an analogy in the interpretation of thermo-mechanical statistics between the entropy-elastic *Gaussian* network and ideal conformational gas, Kilian and Vilgis [25–29] developed the *Van der Waals* strain energy function. The function describes the *Gaussian* network chains as equivalent to the equipartition of energy within a *Van der Waals* conformational gas with weak interactions, mathematically expressed as below.

$$W^{Van-der-Waals} = (Nk_bT)\left\{ -(\lambda_m^2 - 3)[\ln(1 - \eta) + \eta] - \frac{2}{3}a\left(\frac{\tilde{I} - 3}{2}\right)^{\frac{3}{2}} \right\} \quad (30)$$

where $\tilde{I} = (1 + \beta)I_1 + \beta I_2$ and $\eta = \sqrt{\frac{\tilde{I} - 3}{\lambda_m^2 - 3}}$

Characterisation of the *Van der Waals* strain energy function required four material parameters to be completely defined. They include:

1. (Nk_bT) denoting the initial shear modulus G of the material.
2. The finite chain extensibility or locking stretch λ_m (corresponding to an infinite strain energy potential when its limiting value is reached, or more precisely when $\tilde{I} \rightarrow \lambda_m^2$).
3. Parameter a characterising the global interaction between 'quasi-particle' of an ideal gas, or the global interaction between chains in the interpretation of a rubber elastic network.
4. Dimensionless constant β represents a linear mixture parameter combining strain invariants I_1 and I_2 into $\tilde{I}$. It should be noted that when $\beta = 0$, the *Van der Waals* potential will depends on the first invariant alone.

Edwards-Vilgis Crosslink-Sliplink Model

Edwards and Vilgis [30, 31] attempted to improve the previously proposed 'tube model' through a detailed treatment of the consequences of entanglements. The authors found that apart from the replica calculation employed by Ball et. al. [23], the strain energy function for a network consisting of both cross-links and slip-links similar to that of 'tube model' can be evaluated through several other methods including (1) *Flory* segment argument, (2) inextensibility limit of a single chain that interpret a chain's maximum locking stretch as the difference between its fully extended length L and the 'primitive path' length of the tube L_{pp} and/or (3) the *Rouse* theory of linear viscoelasticity [32] (the readers are referred to the literatures [30, 31, 33, 34] for further details in each of these concepts). The resulting unit volume strain energy function involves an additional parameter α, which measure the inextensibility λ_{max} (corresponding to a singularity in stress) of the network chains ($\alpha = 1/\lambda_{max}$), expressed in the form given below

$$W^{Edwards-Vilgis} = W_{CL} + W_{SL} \tag{31}$$

where the strain energy contribution from cross-links W_{CL} is

$$W_{CL} = \frac{1}{2}(N_c k_B T) \left[\frac{\sum\limits_{i=1}^{3}(1-\alpha^2)\lambda_i^2}{1-\alpha^2\sum\limits_{i=1}^{3}\lambda_i^2} + \ln\left(1-\alpha^2\sum\limits_{i=1}^{3}\lambda_i^2\right) \right] \tag{32}$$

and the strain energy contribution as a result of entanglement or slip-links is

$$W_{SL} = \frac{1}{2}(N_s k_B T) \left\{ \sum\limits_{i=1}^{3}\left[\frac{(1+\eta)(1-\alpha^2)\lambda_i^2}{\left(1-\alpha^2\sum\limits_{i=1}^{3}\lambda_i^2\right)(1+\eta\lambda_i^2)} + \ln\left(1+\eta\lambda_i^2\right)\right] + \ln\left(1-\alpha^2\sum\limits_{i=1}^{3}\lambda_i^2\right) \right\} \tag{33}$$

The material's constants N_c, N_s, and η are as defined in Eq. 29. It should be noted that under the extreme case where $\eta = 0$, the energy contribution from slip-links (Eq. 33) returns a form similar to that of the cross-links contribution (Eq. 32). Under such an extreme case, there is no chain slippage allowed in the entire network and the entanglements act as permanent cross-links.

Sweeney-Ward Model

In the work of Sweeney and Ward [35–37], the authors observed that a necking phenomenon routinely occurred in the drawing of semi-crystalline PP and subsequently proposed the modelling of such instabilities by exploiting a modified version of the '*tube*' model. In a uniaxial stretching simulation of PP incorporating the 'tube' theory, it was found that the model successfully captured the many features of the empirical data. However, the model could not reproduce the onset of necking at extension ratios λ less than ≈ 1.8; in reality empirical results had shown that the necking of PP initiated at λ as early as ≈ 1.3. In order to allow the modelling of the onset of necking at a strain comparable to those observed experimentally, a modification was proposed such that as deformation proceeds, interaction between sliplinks in the immediate neighbourhood may lead to a decrease in the sliplinks number N_s. This has been done by making the previously constant sliplink number N_s dependent on the first invariant of strain I_1

$$N_s = \frac{N_{s0} - N_{sf}}{(I_1 - 2)^{\beta}} + N_{sf} \tag{34}$$

where N_{s0} and N_{sf} are constants corresponding to the initial and ultimate sliplink numbers respectively ($N_{sf} \leq N_s \leq N_{s0}$), and β is simply an additional fitting parameter that controls the rate of decay of N_s.

Assuming incompressibility and expressing the three principal stretch ratios λ_1, λ_2, λ_3 in terms of the three invariants of strain I_1, I_2 and I_3, the strain energy function of the 'tube' theory can be rewritten as

$$\frac{W}{k_B T} = \frac{N_c}{2} I_1 + \frac{N_s}{2} \left[\frac{(1+\eta)(I_1 + 2\eta I_2 + 3\eta^2)}{1 + \eta I_1 + \eta^2 I_2 + \eta^3} + \ln\left(1 + \eta I_1 + \eta^2 I_2 + \eta^3\right) \right] \quad (35)$$

It should be noted that in the evaluation of stress, the expressions $(\partial W/\partial I_1)$ and $(\partial W/\partial I_2)$ were first obtained by treating N_s as constant. The varying N_s function (as shown in Eq. 34) entered into the proposed model through the differentiated functions of $(\partial W/\partial I_1)$ and $(\partial W/\partial I_2)$.

3.4 Characterisation of Material Models

The behaviour of a particular polymeric system might well be described by a specific model but not the others. The effectiveness of the chosen material models were assessed in terms of their accuracy in predicting the experimental material behaviour of the PP and HIPS used. The characterisations were carried out through a nonlinear least square fit procedure where the sum of square of the error measure, E, is to be minimised.

$$E = \sum_{i=1}^{N} \left(\sigma_i^{test} - \sigma_i^{th} \right)^2 \quad (36)$$

where N is the number of experimental true stress-stretch ratio data pairs, σ_i^{test} is true stress value from experimental data and σ_i^{th} is model generated true stress.

A number of assumptions were adopted in the evaluation process:

1. The material is assumed to be fully incompressible, i.e. the volume of the material cannot change throughout the deformation process ($\lambda_1 \cdot \lambda_2 \cdot \lambda_3 = 1$).
2. The material is assumed to be homogeneous and isotropic.
3. The material is assumed to be perfectly elastic up to large strain.
4. All nonlinear least square fitting were performed on experimental CW and EB deformation data of PP (at 150 °C, 2 s^{-1}) and HIPS (at 130 °C, 2 s^{-1}).
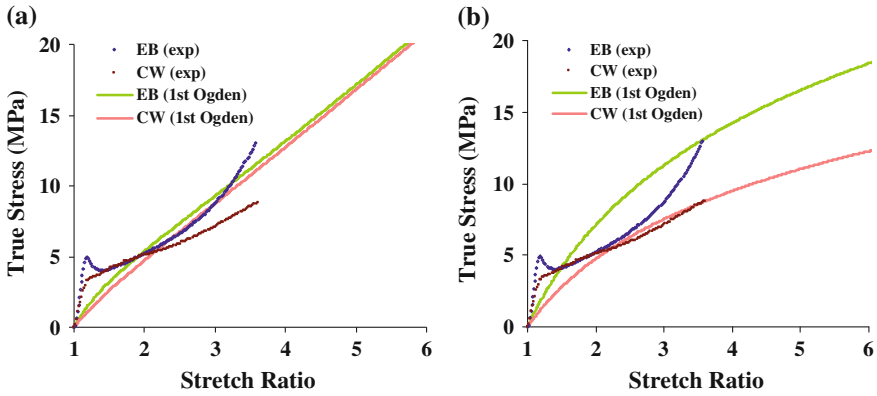
Fig. 6 Model prediction (1st order *Ogden*) to EB and CW responses of PP. **a** Fitted to equal biaxial test data. **b** Fitted to constant width test data
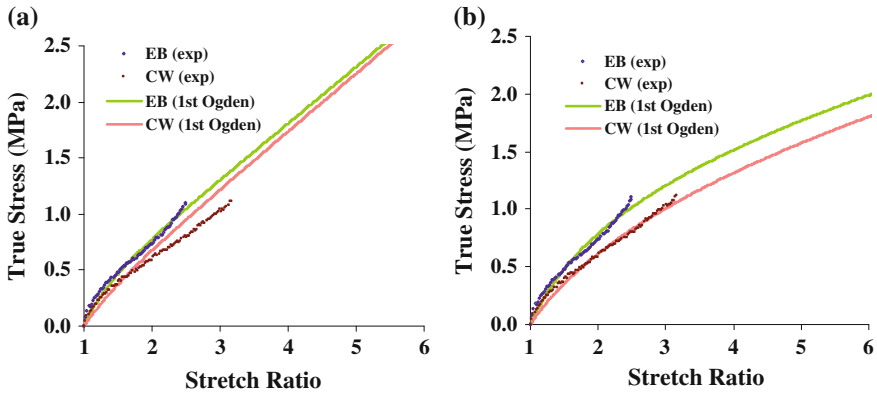
Fig. 7 Model prediction (1st order *Ogden*) to EB and CW responses of HIPS. **a** Fitted to equal biaxial test data. **b** Fitted to constant width test data

# 4 Results and Discussions

4.1 Phenomenological Hyperelastic Model

4.1.1 Ogden Model

The 1st order *Ogden* model was least-square fitted to both EB and CW data of PP and HIPS. Figures 6 and 7 show the fitted results of the 1st order Ogden model.

While the 1st order Ogden model predict relatively well the deformation behaviour of HIPS, the model failed to capture the deformation response of the PP. It can be observed that a higher order terms (2nd order Ogden model) introduced

(a)

(b)
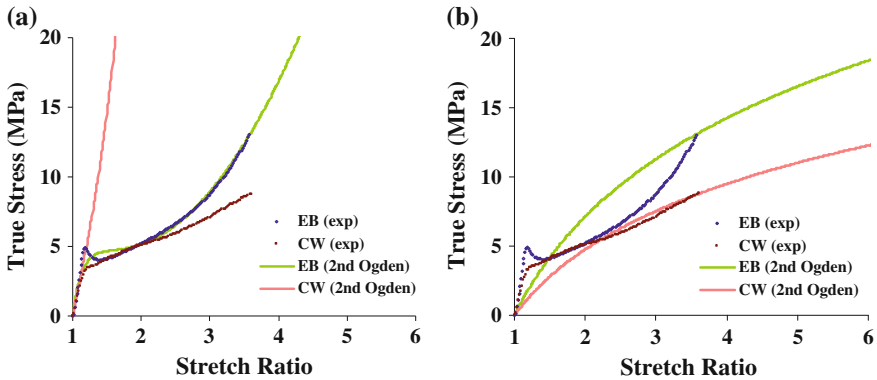
Fig. 8 Model prediction (2nd order *Ogden*) to EB and CW responses of PP. **a** Fitted to equal biaxial test data. **b** Fitted to constant width test data

(a)

(b)
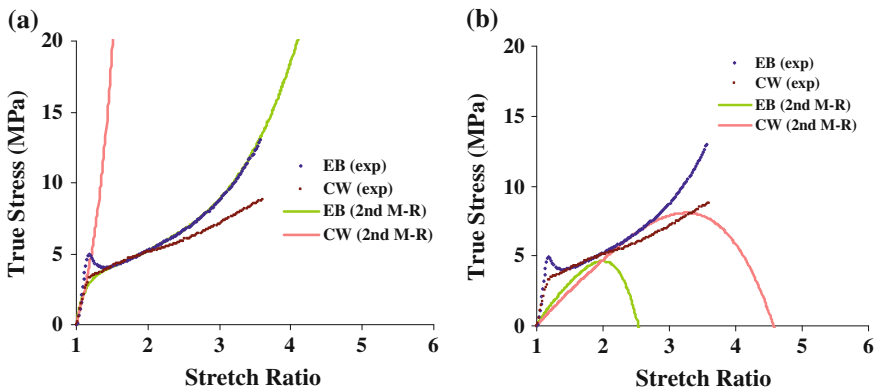
Fig. 9 Model prediction (2nd order M-R) to EB and CW responses of PP. **a** Fitted to equal biaxial test data. **b** Fitted to constant width test data

greater nonlinearity into the model simulated true stress-stretch ratio curves, Fig. 8, as expected. However, the model revealed an unrealistic material response in constant width deformation (i.e. deformation stress much higher than in equal biaxial and the stress heads towards infinity in constant width deformation).

4.1.2 Mooney-Rivlin Model

Figures 9 and 10 depict the fitted results of the 2nd order Mooney-Rivlin model to PP and HIPS, respectively.

It can be seen that with the use of material parameters fitted from EB test data, the 2nd order *Mooney-Rivlin* model show a good agreement (apart from the pronounced yielding and strain softening exhibited by PP) between model
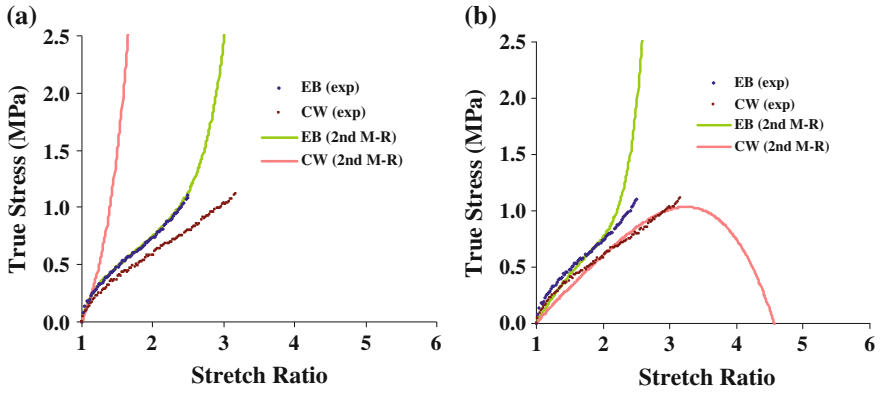
Fig. 10 Model prediction (2nd order M-R) to EB and CW responses of HIPS. **a** Fitted to equal biaxial test data. **b** Fitted to constant width test data

predicted EB response and the experimental results of both PP and HIPS, however, its reveals an unrealistic material response in constant width deformation. Employing the material parameters fitted from CW test data, the 2nd order *Mooney-Rivlin* model again shows a non-physical result for PP where the model revealed a dramatic decrease in tensile stress (towards negative) with the increase in stretch ratio above 2 (in EB) and 3.5 (in CW).

4.2 Physical Network Hyperelastic Model

4.2.1 neo-Hookean Model

Figures 11 and 12 show the fitted results of the neo-Hookean model to PP and HIPS, respectively. It was found that the *neo-Hookean* (*Gaussian* network) model is incapable of capturing the EB and CW deformation behaviour of both PP and HIPS used in this study. In addition, the model simulated EB and CW true stress-stretch ratio curves are observed to be nearly identical.

4.2.2 Three-Chain Model

The 4th-term extension of the inverse *Langevin* function was employed in the evaluation of the true stress-stretch ratio relationship of the 3-*chain* model. Figures 13 and 14 show the fitted results of the 3-chain model to PP and HIPS, respectively. It can be observed that the *non-Gaussian* 3-*chain* model is incapable of capturing the equal biaxial and constant width deformation of both PP and HIPS used in this study. In addition, the model prediction was found to be very similar to the *neo-Hookean Gaussian* network model.
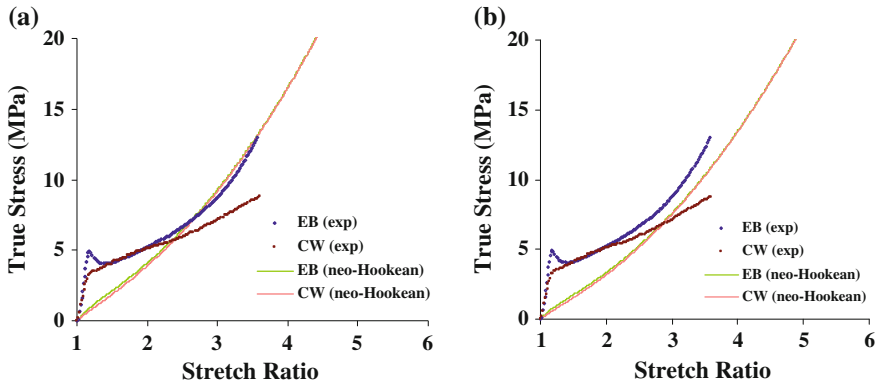
(a)

(b)

Fig. 11 Model prediction (neo-Hookean) to EB and CW responses of PP. **a** Fitted to equal biaxial test data. **b** Fitted to constant width test data
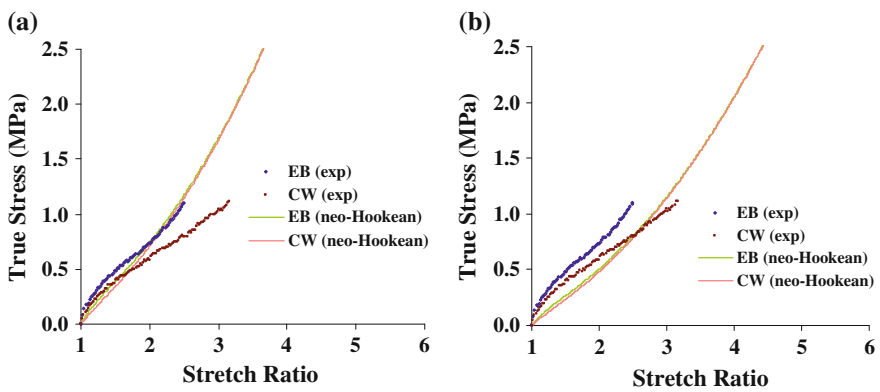
(a)

(b)

Fig. 12 Model prediction (neo-Hookean) to EB and CW responses of HIPS. **a** Fitted to equal biaxial test data. **b** Fitted to constant width test data
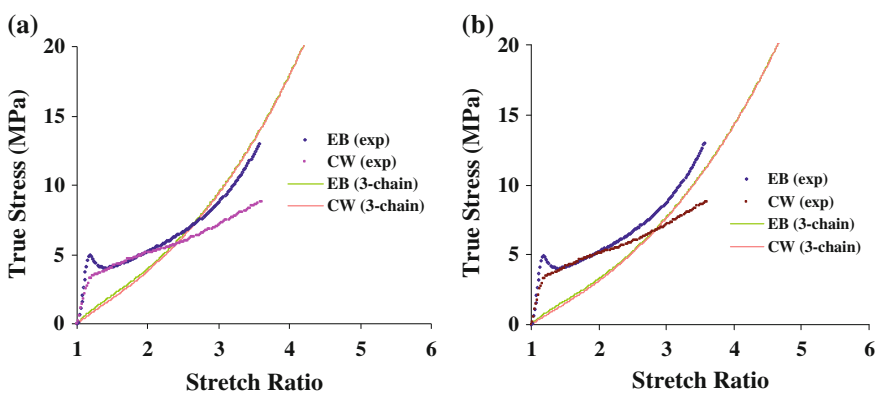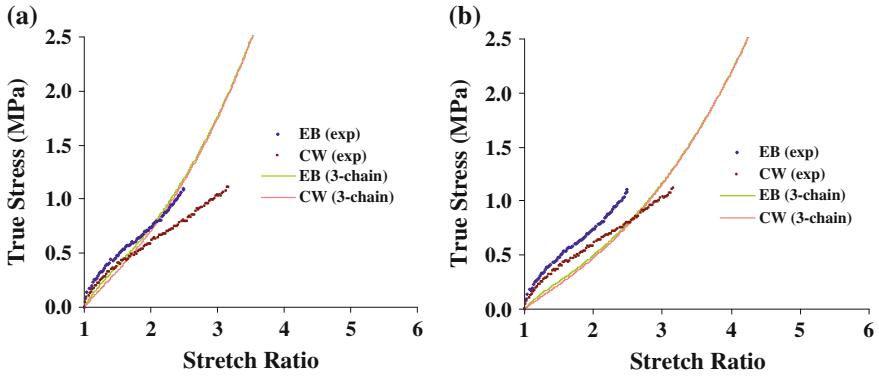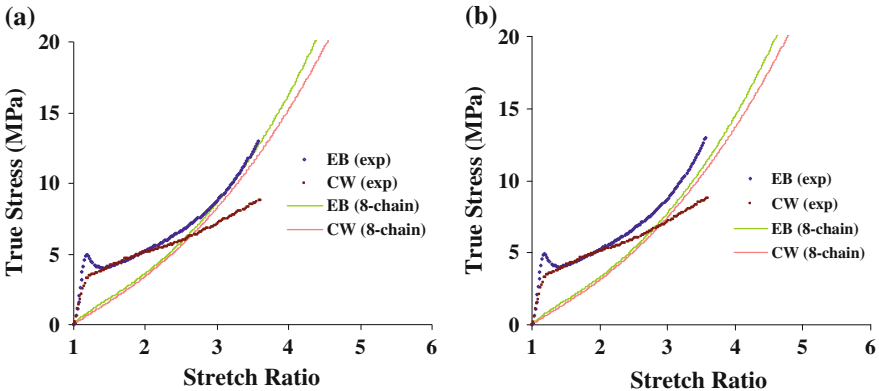
(a)

(b)

Fig. 13 Model prediction (3-chain model) to EB and CW responses of PP. **a** Fitted to equal biaxial test data. **b** Fitted to constant width test data
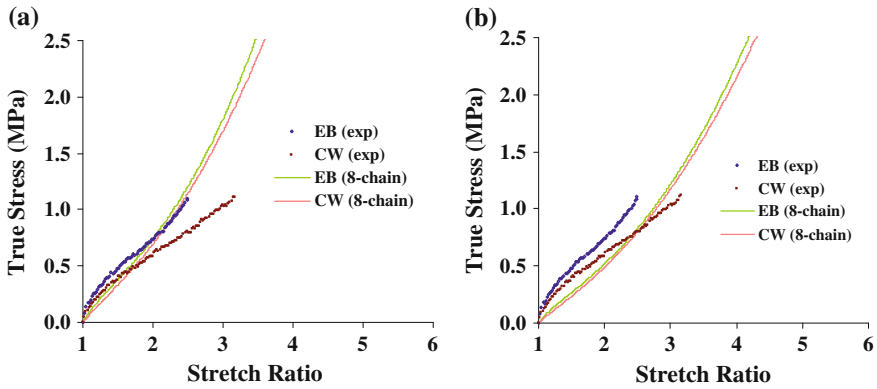
Fig. 14 Model prediction (3-chain model) to EB and CW responses of HIPS. **a** Fitted to equal biaxial test data. **b** Fitted to constant width test data
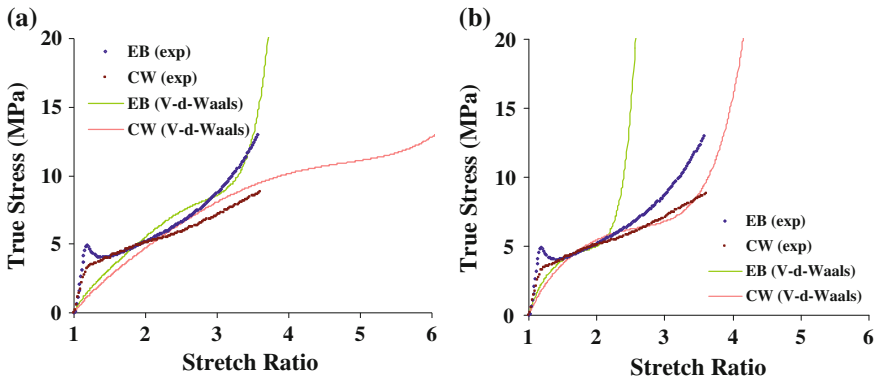

Fig. 15 Model prediction (8-chain model) to EB and CW responses of PP. **a** Fitted to equal biaxial test data. **b** Fitted to constant width test data

4.2.3 Eight-Chain Model

Similar to the prediction of the *neo-Hookean* (*Gaussian* network) and 3-*chain* (*non-Gaussian* network) models, the *non-Gaussian* 8-*chain* model was found incapable of accurately simulating the EB and CW deformation behaviour of both PP and HIPS used in this study, as shown in Figs. 15 and 16. The 4th-term extension of the inverse *Langevin* function was employed in the evaluation of the true stress-stretch ratio relationship of the 8-*chain* model.

Fig. 16 Model prediction (8-chain model) to EB and CW responses of HIPS. **a** Fitted to equal biaxial test data. **b** Fitted to constant width test data
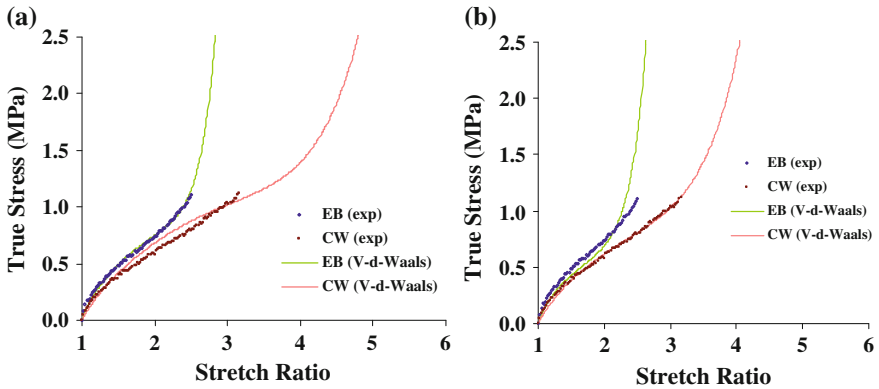

Fig. 17 Model prediction (Van der Waals) to EB and CW responses of PP. **a** Fitted to equal biaxial test data. **b** Fitted to constant width test data
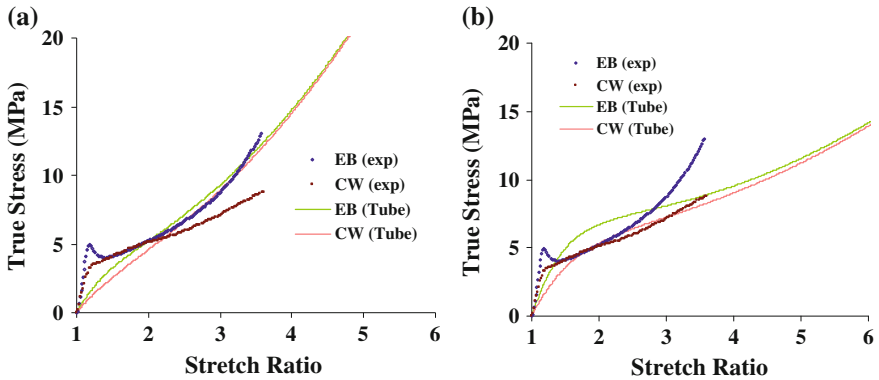
4.2.4 Van der Waals Model

Figures 17 and 18 show the fitted results of the Van der Waals model to PP and HIPS, respectively. It can be observed that although the *Van der Waals* model gives a better representation of the deformation behaviour of PP compared to the *Gaussian* (*neo-Hookean*) and *non-Gaussian* (*3-chain*, *8-chain*) network model, the accuracy of the model prediction is relatively poor. The simulated EB stress moves towards infinity at a stretch ratio found to be too low for finite element simulation of typical deep draw free surface moulding processes. On the other hand, the simulated true stress-stretch ratio curves of the *Van der Waals* model were found to be comparable to the experimental data of HIPS. In all cases, the least-square fit

Fig. 18 Model prediction (Van der Waals) to EB and CW responses of HIPS. **a** Fitted to equal biaxial test data. **b** Fitted to constant width test data
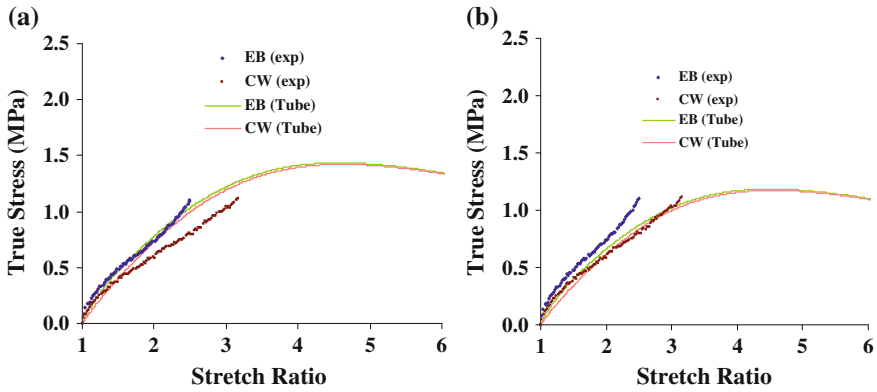

Fig. 19 Model prediction (Ball 'tube' model) to EB and CW responses of PP. **a** Fitted to equal biaxial test data. **b** Fitted to constant width test data

of the *Van der Waals* model parameters reveals that the simulated true stress-stretch ratio curve is very sensitive to slight changes in each of its material parameters, especially parameter β.

4.2.5 Ball "Tube" Model

From the nonlinear least-square fit results of *Ball* model, it can be observed that the model was unsuccessful in simulating the deformation behaviour of both PP and HIPS used in this study, as shown in Figs. 19 and 20 respectively. For PP, the simulated curves were virtually similar for both EB and CW deformation. For HIPS, it was observed that the optimal least-square fitted parameters produced

(a)

(b)

Fig. 20 Model prediction (Ball 'tube' model) to EB and CW responses of HIPS. **a** Fitted to equal biaxial test data. **b** Fitted to constant width test data
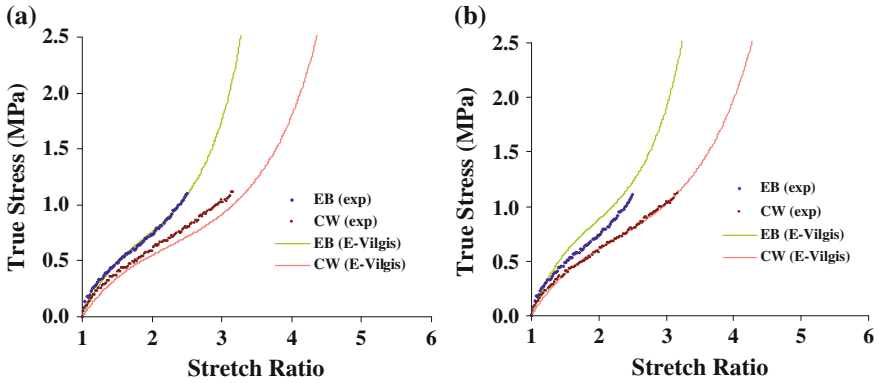
(a)

(b)
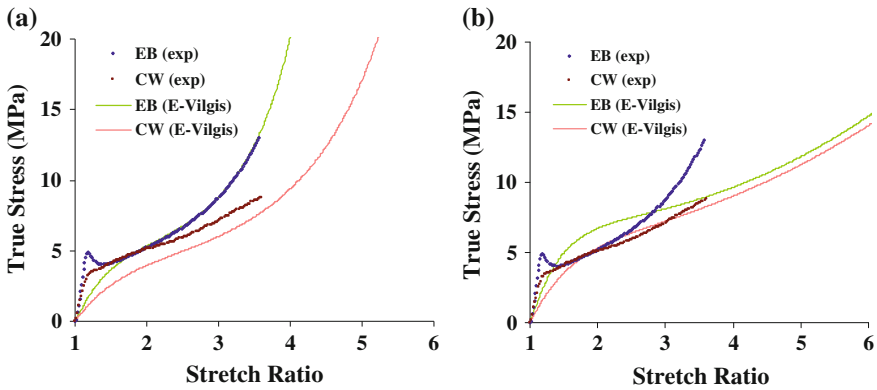
Fig. 21 Model prediction (Edwards-Vilgis) to EB and CW responses of PP. **a** Fitted to equal biaxial test data. **b** Fitted to constant width test data

stresses, which tend to drop with increasing stretch ratio, indicating the onset of the model's instability at large stretch.

### 4.2.6 Edwards-Vilgis Crosslink-Sliplink Model

Figures 21 and 22 show the fitted results of the Edwards-Vilgis model to PP and HIPS, respectively.

When material constants best fitted to experimental EB data are used, the *Edwards-Vilgis* model was found capable of accurately simulating the EB deformation responses of both PP (apart from the significant yielding found in the test
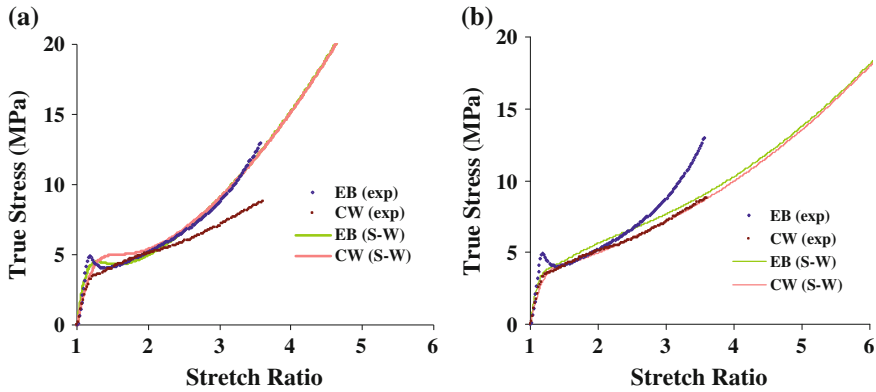
Fig. 22 Model prediction (Edwards-Vilgis) to EB and CW responses of HIPS. **a** Fitted to equal biaxial test data. **b** Fitted to constant width test data

Fig. 23 Model prediction (Edwards-Vilgis) to EB and CW responses of HIPS. (Averaging material constant fitted from EB and CW)
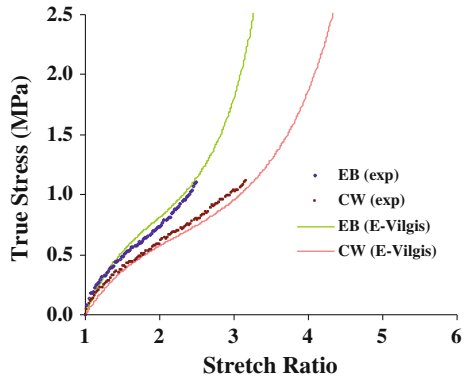
data) and HIPS. However, the model under-predicted the true stress in CW deformation of PP. In the case of HIPS, only a slight discrepancy was found in the simulated constant width curve. When material constants best fitted to experimental CW data are used, the model not only gives unacceptable prediction in the equal biaxial curve, but also under predicts both the initial modulus and strain hardening in the constant width curve.

The slight discrepancy observed in the model predicted response of HIPS may be attributed to the minor variation in experimental data. Alternatively, an average of the characterised constants from both EB and CW test data of HIPS can be evaluated to give higher accuracy in the simulated responses, as shown in Fig. 23.
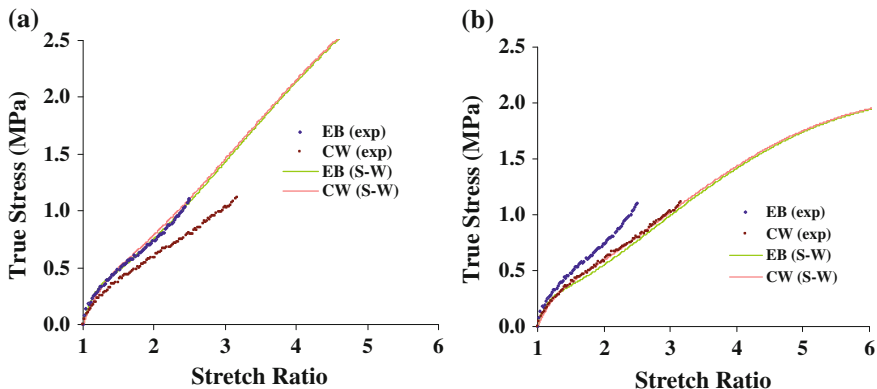
(a)

(b)

Fig. 24 Model prediction (Sweeney-Ward) to EB and CW responses of PP. **a** Fitted to equal biaxial test data. **b** Fitted to constant width test data

4.2.7 Sweeney-Ward Model

The model was proposed as a modified form of the *Ball* model, where the sliplink constant N_s was made dependent on the first strain invariant to allow the number of sliplink N_s to decrease with increasing strain. This modification resulted in a constitutive function that is no longer hyperelastic (since the strain energy has been made dependent on the deformation path and a strain energy function does not exist), but remains elastic in the *Cauchy* sense (since stress depends only on the current state of strain and no rate dependency is accounted for). Therefore, the resulting constitutive function of *Sweeney-Ward* no longer obeys the theory of energy conservation. In fact, the authors [37] did point out that the proposed model is liable to the objection where by loading via a deformation path and unloading through a different one, the material model may acquire more work on unloading than was required to load it. The cause of the problem was attributed to the implicit assumption that the sliplink number N_s will essentially recover to its original value on unloading, however in practice, the deformation is expected to have permanent effects.

The entire experimental equal biaxial true stress-stretch ratio data of PP, including the yield and strain softening were used in the least-square fit procedure for the *Sweeney-Ward* model. Figures 24 and 25 show the fitted results of the *Sweeney-Ward* model to PP and HIPS, respectively. When material constants best fitted to EB test data are used, it can be observed that the model is capable of accurately representing the equal biaxial deformation response of both PP and HIPS. However, the model simulated CW response was found to be virtually identical to that of the EB deformation. A similar trend is observed when the model is fed with material constants characterised from constant width test data.

It should be noted that in the nonlinear least-square fitting procedure of the *Ball*, *Edwards-Vilgis* and *Sweeney-Ward* models, the material constant corresponding to

Fig. 25 Model prediction (Sweeney-Ward) to EB and CW responses of HIPS. **a** Fitted to equal biaxial test data. **b** Fitted to constant width test data

the number of crosslink N_c was assigned to 0 for HIPS, due to the fact that HIPS is an amorphous non-crosslinked material and its modulus is assumed to be contributed by chain entanglements or sliplinks alone. For the PP, the appearance of the crystalline phase was assumed to act as artificial crosslinks within the material. This can be attributed to the fact that at forming temperature, the mobility of the amorphous phase is much higher than the crystalline phase, due to the fact that the solid phase forming temperature of PP is far higher than its glass transition temperature (T_g at $\approx -5\,°C$ as determined from DMTA) and thus the modulus is assumed to be contributed from both crosslink and sliplink.

Quantitative fit of the hyperelastic or *Cauchy's* elastic models investigated in this work can be visualised by evaluating the 'root mean square error' between the model's prediction and the experimental data through

$$RMSE = \left[\frac{1}{N} \cdot \sqrt{\sum_{i=1}^{N} \left(\sigma_i^{test} - \sigma_i^{model}\right)^2}\right] \tag{37}$$

where N is the number of experimental true stress-stretch ratio data pairs, σ_i^{test} is the true stress value from test data and σ_i^{model} is the model generated true stress.

When fitted to either experimental EB or CW data, the 'root mean square error' of the models' prediction can be shown in Table 1.

It should be noted that while the values of the 'root mean square error' represents the goodness of fit to either experimental EB or CW data, they do not represent the quantitative fit of the models to both deformation modes (e.g. a material model might accurately capture EB deformation but poorly predict the CW response).

Table 1 'RMSE' between models' prediction and experimental data

Constitutive material model	Root mean square error (MPa)			
	Fitted to PP test data		Fitted to HIPS test data	
	EB	CW	EB	CW
1st order *Ogden*	0.0951	0.0728	0.0045	0.0029
2nd order *Ogden*	0.0306	0.0728	–	–
1st order *Mooney-Rivlin*	0.1080	0.1481	0.0047	0.0106
2nd order *Mooney-Rivlin*	0.0402	0.0919	0.0016	0.0047
Neo-Hookean	0.1260	0.1481	0.0086	0.0106
3-chain	0.1333	0.1545	0.0092	0.0114
8-chain	0.1410	0.1513	0.0095	0.0110
Van der Waals	0.0920	0.0449	0.0026	0.0017
Ball 'tube'	0.0879	0.0508	0.0045	0.0037
Edwards-Vilgis	0.0744	0.0507	0.0033	0.0017
Sweeney-Ward	0.0252	0.0101	0.0017	0.0011

5 Conclusions

From the analyses carried out on a range of constitutive hyperelastic models (both phenomenological and physical), it is observed that the simulated true stress-stretch ratio curves from the *Ogden*, *Van der Waals* and *Edwards-Vilgis* models are in reasonably good agreement with the experimental EB and CW deformation behaviour of amorphous HIPS. However, the material models considered in this work were generally incapable of accurately capturing the deformation behaviour of PP, especially in terms of simulating the initial *Young's* modulus, yield and strain softening. In this respect, further development would be required to develop a new constitutive material model that can accurately capture the complex deformation behaviour of PP.

References

1. Hooke, R., De Potentia Restitutiva or of Spring Explaining the Power of Springing Bodies, p. 23. London (1678)
2. Markovitz, H.: The emergency of rheology. Physics Today (American Institute of Physics) **21**(4), 23–33 (1968)
3. Truesdell, C.A., Cauchy's First Attempt at Molecular Theory of Elasticity, Bollettino di Storia delle Scienze Matematiche. Il Giardino di Archimede **1**(2), 133–143 (1981)
4. Bogolyubov, A.N., Augustin Cauchy and His Contribution to Mechanics and Physics (Russian), Studies in the History of Physics and Mechanics, pp. 179–201. Nauka, Moscow (1988)
5. Dahan-Dalmédico, A., La Propagation Des Ondes En Eau Profonde Et Ses Développements Mathématiques (Poisson, Cauchy, 1815–1825), in The History of Modern Mathematics II, pp. 129–168. Boston, MA (1989)

6. Truesdell, C.A.: Cauchy and the modern mechanics of continua. Rev. Hist. Sci. **45**(1), 5–24 (1992)
7. Mooney, M.: A theory of large elastic deformation. J. Appl. Phys. **11**(9), 582–592 (1940)
8. Rivlin, R.S.: Large elastic deformations of isotropic materials, I, II, III, fundamental concepts. Philos. Trans. R. Soc. Lond. Ser. A **240**, 459–525 (1948)
9. Rivlin, R.S.: Large elastic deformations of isotropic materials, IV, further developments of the general theory. Philos. Trans. R. Soc. Lond. Ser. A **241**(835), 375–397 (1948)
10. Ogden, R.W., Large deformation isotropic elasticity: on the correlation of theory and experiment for incompressible rubberlike solids. In: Proceedings of the Royal Society of London, Series A, Mathematical and Physical Sciences, vol. 365, pp. 565–584 (1972)
11. Treloar, L.R.G.: Stress-strain data for vulcanized rubber under various types of deformation. Trans. Faraday Soc. **40**, 59–70 (1944)
12. Ward, I.M., Mechanical Properties of Solid Polymers, 2nd edn. Wiley, Hoboken (1983)
13. Treloar, L.R.G.: The elasticity of a network of long chain molecules I. Trans. Faraday Soc. **39**, 36–64 (1943)
14. Treloar, L.R.G.: The elasticity of a network of long chain molecules II. Trans. Faraday Soc. **39**, 241–246 (1943)
15. Kuhn, W., Grun, F.: Beziehungen zwichen elastischen Konstanten und Dehnungsdoppelbrechung hochelastischer stoffe. Kolloideitschrift **101**, 248–271 (1942)
16. James, H.M., Guth, E.: Theory of elastic properties of rubber. J. Chem. Phys. **11**(10), 455–481 (1943)
17. Wang, M.C., Guth, E.: Statistical theory of networks of non-gaussian flexible chains. J. Chem. Phys. **20**, 1144–1157 (1952)
18. Arruda, E.M., Boyce, M.C.: A three-dimensional constitutive model for the large stretch behavior of rubber elastic materials. J. Mech. Phys. Solids **41**(2), 389–412 (1993)
19. Treloar, L.R.G., Riding, G., A non-gaussian theory for rubber in biaxial strain I, mechanical properties. In: Proceedings of the Royal Society of London, Series A, Mathematical and Physical Sciences, vol. 369, pp. 261–280 (1979)
20. Wu, P.D., Van der Giessen, E.: On improved 3-D non-Gaussian network models for rubber elasticity. Mech. Res. Commun. **19**(5), 427–433 (1992)
21. Wu, P.D., Van der Giessen, E.: On improved network models for rubber elasticity and their applications to orientation hardening in glassy polymers. J. Mech. Phys. Solids **41**(3), 427–456 (1993)
22. Flory, P.J., Erman, B.: Theory of elasticity of polymer networks. Macromolecules **15**(3), 800–806 (1982)
23. Ball, R.C., Doi, M., Edwards, S.F., Warner, M.: Elasticity of entangled networks. Polymer **22**(8), 1010–1018 (1981)
24. Doi, M., Edwards, S.F.: The theory of polymer dynamics. Oxford University Press, Oxford (1986)
25. Kilian, H.G.: Equation of state of real networks. Polymer **22**, 209–217 (1981)
26. Kilian, H.G.: Energy balance in networks simply elongated at constant temperature. Colloid Polym. Sci. **259**, 1084–1091 (1981)
27. Vilgis, T.H., Kilian, H.G.: The van der waals-network—a phenomenological approach to dense networks. Polymer **25**, 71–74 (1984)
28. Kilian, H.G., Vilgis, T.H.: Fundamental aspects of rubber-elasticity in real networks. Colloid Polym. Sci. **262**, 15–21 (1984)
29. Kilian, H.G.: An interpretation of the strain-invariants in largely strained networks. Colloid Polym. Sci. **263**, 30–34 (1985)
30. Edwards, S.F., Vilgis, T.H.: The effect of entanglements in rubber elasticity. Polymer **27**(4), 483–492 (1986)
31. Edwards, S.F., Vilgis, T.H.: The stress-strain relationship in polymer glasses. Polymer **28**(3), 375–378 (1987)
32. Rouse, P.E.: A theory of the linear viscoelastic properties of dilute solutions of coiling polymers. J. Chem. Phys. **21**, 1272–1280 (1953)

33. Flory, P.J.: Principles of Polymer Chemistry. Cornell University Press, New York (1966)
34. Flory, P.J.: Theory of Polymer Networks. The Effect of Local Constraints on Junctions. J. Chem. Phys. **66**(12), 5720 (1977)
35. Sweeney, J., Ward, I.M.: The modeling of multiaxial necking in polypropylene using a sliplink-crosslink theory. J. Rheol. **39**(5), 861–872 (1995)
36. Sweeney, J., Kakadjian, S., Craggs, G., Ward, I.M., The multiaxial stretching of polypropylene at high temperatures. In: ASME Mechanics of Plastics and Plastic Composites, MD vol. 68 / AMD vol. 215 pp. 357–364 (1995)
37. Sweeney, J., Ward, I.M.: A constitutive law for large deformations of polymers at high temperatures. J. Mech. Phys. Solids **44**(7), 1033–1049 (1996)